

# The equation of state of QCD at finite chemical potential

Sourendu Gupta\* and Nikhil Karthik†

*Department of Theoretical Physics,  
Tata Institute of Fundamental Research,  
Homi Bhabha Road, Mumbai 400005, India.*

Pushan Majumdar‡

*Department of Theoretical Physics, Indian Association for the Cultivation of Science,  
Raja Subodh Chandra Mallick Road, Jadavpur, Kolkata 700032, India.*

We obtain the baryon number density,  $n$ , and the excess contribution to the pressure,  $\Delta P$ , at finite chemical potential,  $\mu_B$ , and temperature,  $T$ , by resumming the Taylor series expansion in a lattice computation with lattice spacing of  $1/(4T)$  and two flavours of quarks at three different quark masses. The method proceeds by giving a critical  $\mu_B$  and limits on the critical exponent, and permits reliable estimations of the errors in resummed quantities. We find that  $n$  and  $\Delta P$  are insensitive to the quark mass. We also report the bulk isothermal compressibility,  $\kappa$ , over a range of  $T$  and  $\mu_B$ .

PACS numbers: 12.38.Mh, 11.15.Ha, 12.38.Gc

## I. INTRODUCTION

Heavy-ion collisions produce hot QCD matter which comes to thermal equilibrium [1]. The resulting fireball evolves. Its evolution is expected to be described with reasonable accuracy within hydrodynamics [2]. As a result, computing the equation of state of QCD matter at values of  $T$  and  $\mu_B$  accessible to colliders is a matter of interest.

A systematic expansion of the pressure,  $P$ , of QCD as a series in  $\mu_B$  was first introduced in order to examine the equation of state at finite chemical potential [3]. The Taylor coefficients of the expansion are the quark number susceptibilities (QNS), the first of which had been introduced and studied long ago [4]. The QNS are of interest in experimental studies of event-to-event fluctuations of conserved quantities [5, 6], and therefore have become important objects of study in recent years. They also indicate a divergence of the series at finite and real  $\mu_B$ , implying the existence of a critical point [7].

The presence of such divergences could be a barrier to extracting the equation of state of QCD. In this paper we examine the summation of these series. We examine techniques of propagating measurement errors and evaluate the change in pressure due to the baryon chemical potential,

$$\Delta P(T, \mu_B) = P(T, \mu_B) - P(T, \mu_B = 0), \quad (1)$$

and the baryon number density,  $n(T, \mu_B)$ . Since the pressure at zero chemical potential,  $P(T, \mu_B = 0)$  is being studied with great precision [8, 9], our work opens the door to the evaluation of pressure over a large part of the phase diagram of relevance to current and near-future experiments. Interestingly, the method can also begin to give more information on the critical behaviour [10].

This study has another interesting ramification.  $\Delta P$  and  $n$  get contributions only from degrees of freedom which carry baryon number— baryons at low temperature, and quarks at high temperature. However, chiral degrees of freedom may be involved through a mixing between the chiral condensate and the baryon number density [11]. If this happens, then the scaling directions at the critical point become mixtures of the physical parameters  $T$ ,  $\mu_B$  and  $m$  (we discuss this point further in Appendix B). In fact, the older literature sometimes discusses the critical point of QCD purely in terms of the chiral order parameter. So it is interesting to check how strongly  $\Delta P$  and  $n$  depend on the quark mass. By performing simulations with three different bare quark masses, we are able to throw some light on these questions. We study the effect of changing quark masses on the position of the critical end point and the equation of state, and find statistically insignificant changes.

---

\*Electronic address: [sgupta@theory.tifr.res.in](mailto:sgupta@theory.tifr.res.in)

†Electronic address: [nikhil@theory.tifr.res.in](mailto:nikhil@theory.tifr.res.in)

‡Electronic address: [tppm@iacs.res.in](mailto:tppm@iacs.res.in)

$\beta$	$T/T_c$	Statistics	$\tau$	$P_s$	$P_t$	$W$	$\langle\bar{\psi}\psi\rangle$
5.34	$0.89 \pm 0.02$	500+10000	15	1.495(3)	1.494(4)	0.041(5)	0.901(4)
5.35	$0.92 \pm 0.02$	500+20000	50	1.509(9)	1.507(7)	0.05(2)	0.87(2)
5.355	$0.94 \pm 0.01$	500+20000	48	1.515(7)	1.513(6)	0.06(2)	0.85(2)
5.36	$0.96 \pm 0.01$	500+40000	74	1.52(1)	1.519(8)	0.06(3)	0.84(3)
5.372	1.00	500+120000	164	1.550(7)	1.545(6)	0.10(1)	0.76(2)
5.39	$1.06 \pm 0.02$	500+5000	125	1.58(1)	1.58(1)	0.15(3)	0.66(5)
5.40	$1.11 \pm 0.01$	500+5000	30	1.596(3)	1.587(2)	0.165(5)	0.626(9)

TABLE I: The set A runs on  $4 \times 16^3$  lattices and fixed  $am = 0.1$ . Four quantities were monitored to determine thermalization and autocorrelations, namely, the spatial plaquette,  $P_s$ , the temporal plaquette,  $P_t$ , the bare Wilson line,  $W$ , and the bare quark condensate,  $\langle\bar{\psi}\psi\rangle$ . The autocorrelation time,  $\tau$ , quoted here is the maximum of the autocorrelations of these four quantities.

$\beta$	$ma$	$T/T_c$	Statistics	$\tau$	$P_s$	$P_t$	$W$	$\langle\bar{\psi}\psi\rangle$
5.20	0.033	$0.75 \pm 0.02$	980+4000	9	1.394(1)	1.393(1)	0.01953(3)	0.9392(1)
5.22	0.03125	$0.80 \pm 0.02$	980+4000	12	1.411(1)	1.410(1)	0.02238(3)	0.9023(7)
5.24	0.0298	$0.85 \pm 0.01$	980+4000	14	1.430(1)	1.429(1)	0.02707(7)	0.856(1)
5.26	0.02778	$0.90 \pm 0.01$	980+4000	20	1.452(2)	1.450(2)	0.0351(1)	0.795(2)
5.275	0.02631	$0.95 \pm 0.01$	980+4000	30	1.472(3)	1.470(3)	0.0494(4)	0.7264(9)
5.2875	0.025	1.00	1980+8000	98	1.503(9)	1.499(8)	0.08(1)	0.60(4)
5.30	0.02380	$1.05 \pm 0.02$	980+4000	32	1.553(3)	1.543(3)	0.149(4)	0.33(2)
5.35	0.02	$1.25 \pm 0.01$	980+4000	6	1.595(1)	1.584(1)	0.1858(6)	0.173(1)
5.425	0.01667	$1.50 \pm 0.01$	980+4000	6	1.6350(4)	1.6240(3)	0.2109(4)	0.1093(2)
5.54	0.0125	$2.04 \pm 0.02$	980+4000	5	1.6830(3)	1.6730(3)	0.2393(3)	0.06630(1)

TABLE II: The set B runs on  $4 \times 16^3$  lattices. Four quantities were monitored to determine thermalization and autocorrelations, namely, the spatial plaquette,  $P_s$ , the temporal plaquette,  $P_t$ , the bare Wilson line,  $W$ , and the bare quark condensate,  $\langle\bar{\psi}\psi\rangle$ . The autocorrelation time,  $\tau$ , quoted here is the maximum of the autocorrelations of these four quantities.

Here is the plan of this paper. In the next section we discuss the simulations and also introduce our notation. The following section is a detailed technical discussion of all our results, a summary of which also appears in the final section. The appendices contain technical details of the analysis of errors on Padé approximants, Widom scaling at the QCD critical point, and the definition of the isothermal compressibility in QCD.

## II. SIMULATIONS AND NOTATION

This study was made on  $4 \times 16^3$  lattices using three sets of configurations, one set each for a different value of  $m_\pi/m_\rho$ , as described next. At zero chemical potential, QCD with massive quarks does not have a phase transition, but a broad crossover. There can be many conventions for defining the crossover temperature [12]. We choose to define it by the peak in the Polyakov loop susceptibility. The peak in the 4th order QNS occurs at the same temperature [13].

The first set of configurations (called set A in this paper) was obtained at  $m_\pi/m_\rho \simeq 0.58$ . Each trajectory was of 1 MD time unit, and used a time step of 0.05 MD time units. After discarding the first 500 trajectories for thermalization, 200 configurations were collected in each simulation. The details are given in Table I. We identified the critical coupling by a multi-histogram reweighting and obtained  $\beta_c = 5.3720 \pm 0.0005$ . This is in agreement with an old MILC result of  $\beta_c = 5.375 \pm 0.020$ , obtained on  $4 \times 8^3$  lattice [4]. At these bare parameters, MILC had made hadron mass measurements which yielded the value of  $m_\pi/m_\rho$  quoted above [14]. Although we do not tune this set to remain at fixed  $m_\pi/m_\rho$ , the variation of  $\beta$  is small enough that the change in this ratio over the whole range is expected to be less than 10%. We measured the temperature scale given in Table I using the method adopted in [7].

The most extensive set of runs we made was meant to extend the study of [7] with more statistics. The run parameters and statistics of this set (set B) are given in Table II. In these simulations we have  $m_\pi/m_\rho \simeq 0.31$ . Each trajectory was of length 2 MD time units, and used a time step of 0.01 MD time units. In each of the runs 980 trajectories were discarded for thermalization. At  $\beta_c = 5.2875$  we collected 100 gauge configurations, one every 80 trajectories, and 200 configurations, one every 20 trajectories, at other values of  $\beta$ . This was sufficient for the stored

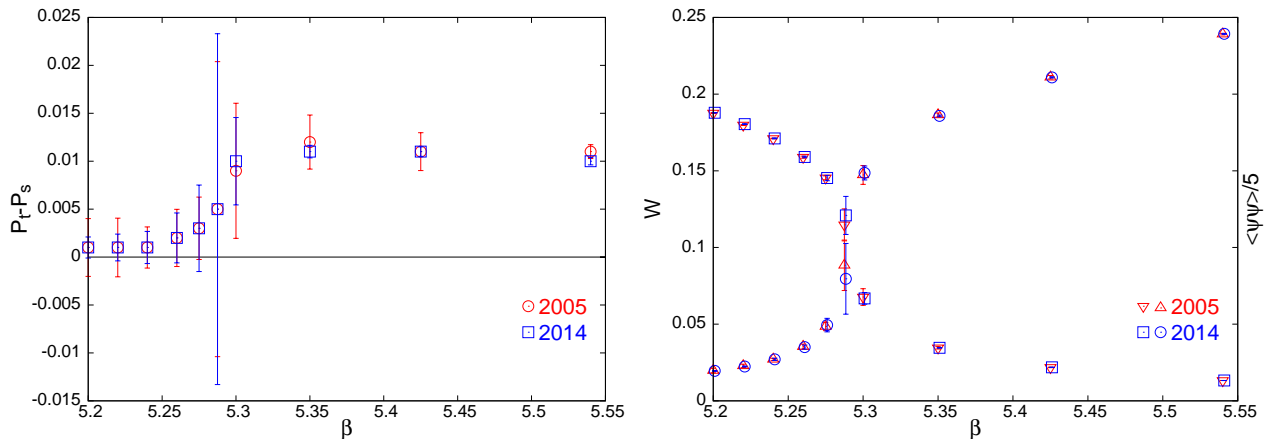


FIG. 1: Basic comparison of the present set B and older [7] runs is made through three quantities which enter thermodynamic variables. The first panel displays the plaquette difference  $P_t - P_s$ . The second panel shows  $W$  (up triangles and circles) and  $\langle \psi \bar{\psi} \rangle$  (down triangles and boxes). The large errors at the cross-over coupling,  $\beta = 5.2875$ , are due to larger autocorrelations. At all couplings the new simulations are compatible with the old, while having smaller errors.

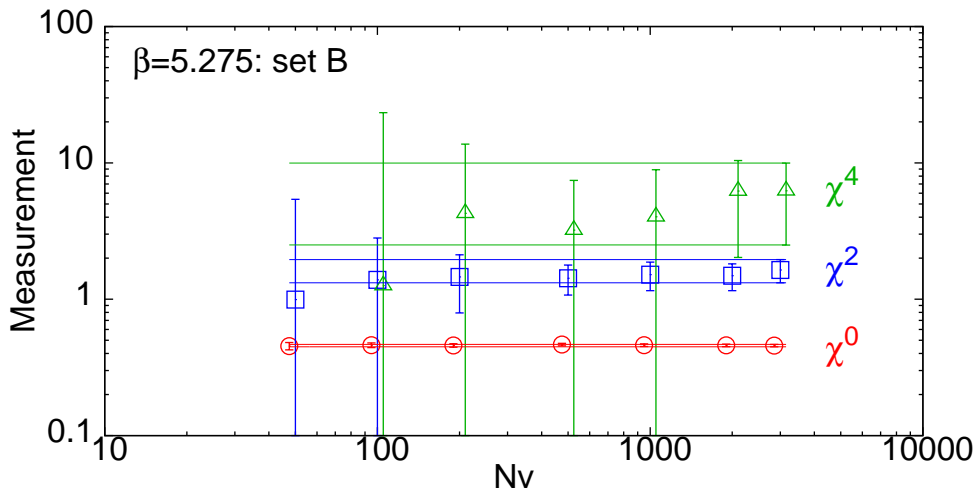


FIG. 2: The number of fermion sources required to control errors in the QNS grows rapidly with the order. The data for  $\chi^0$  has been displaced to the left by 5% and that for  $\chi^4$  to the right by 5%. For the second order QNS,  $\chi^0$ , it is sufficient to take 50 sources, whereas for the 6th order QNS,  $\chi^4$ , one needs at least 2000 source vectors.

configurations to be statistically independent. We checked that the global thermodynamic variables in this run are fully consistent with those in [7]. These checks are shown in Figure 1. The scale setting has been discussed earlier [7], and we use those results to write a temperature scale corresponding to the bare parameters at which we simulated.

The third set of configurations we used has been described in [13], where it was called set N. In this paper we call this the set C. For this set  $m_\pi/m_\rho \simeq 0.25$  [13]. With about 50–60 configurations, this has lower statistics than the other sets. However, we used up to 2000 source vectors at several couplings. In order to understand the effects of statistics, we supplemented it by a sample of 400 independent configurations at  $\beta = 5.255$  and  $am = 0.0165$ , corresponding to  $T/T_c = 0.93 \pm 0.01$ . The mass measurements as well as the determination of the temperature scale was reported in [13].

Another difference between this and earlier measurements [7] is the number of fermion sources,  $N_v$ , used to perform traces over fermion loops. The  $n$ -th order QNS contain up to  $n$  loops. We show in Figure 2 that  $N_v = 50$  seems to suffice for accurate measurements of second order QNS, but the sixth order requires  $N_v = 2000$ . At  $\beta = 5.275$  we checked using  $N_v = 3000$  that the difference between using  $N_v = 2000$  and this larger number of sources is statistically insignificant. So in the rest of the measurements below  $T_c$  we used  $N_v = 2000$ . Above  $T_c$  the measurements turn out to be much less noisy, and we used  $N_v = 1000$ , although it seems that about half this number of sources is sufficient for our purposes. The importance of using large  $N_v$  was first pointed out in [15].

In Figure 3 we compare the earlier [7] and current results. Clearly the increased statistics leads to reduced errors, as expected, and also a much smoother variation of results with  $T$ . The most noticeable change is that the height of the peak in  $\chi_{40}$  is almost half of its earlier value. By varying  $N_v$  and the number of configurations used in our analysis, we found that this was caused by low statistics.

Many of the measurements we perform involve variables whose distributions are non-Gaussian, and sometimes skewed [16]. All the statistical analysis in this paper therefore uses the bootstrap procedure, which yields non-parametric estimators of means and errors. When the distribution is strongly skewed, the error estimators may be non-symmetric; in such cases we quote different upper and lower error bars.

The notation we use in this paper is collected here. The derivatives of the excess pressure give the baryon number density and the baryon number susceptibility, respectively,

$$n(T, \mu_B) = \frac{\partial \Delta P(T, \mu_B)}{\partial \mu_B} \quad \text{and} \quad \chi_B(T, \mu_B) = \frac{\partial^2 \Delta P(T, \mu_B)}{\partial \mu_B^2}. \quad (2)$$

The Taylor expansion of  $\Delta P$  at vanishing  $\mu_B$  is

$$\frac{\Delta P(T, \mu_B)}{T^4} = \frac{\chi_B^2(T)}{T^2} \frac{\mu_B^2}{2!T^2} + \chi_B^4(T) \frac{\mu_B^4}{4!T^4} + \chi_B^6(T) T^2 \frac{\mu_B^6}{6!T^6} + \dots. \quad (3)$$

The Taylor coefficients are the QNS evaluated at  $\mu_B = 0$ ; only the even coefficients survive at this symmetric point. We will often write  $\chi_B$  instead of  $\chi_B^2$ ; no confusion is caused by this. This Taylor series gives rise to those for  $n$  and  $\chi_B$ . We work with two flavours of light degenerate dynamical quarks, so there are in fact two different conserved quark numbers, one for each flavour. One can write a double Taylor series expansion

$$\frac{\Delta P(T, \mu_B)}{T^4} = \sum_{mn} \frac{1}{m!n!} \chi_{mn}(T) T^{m+n-4} \left(\frac{\mu_u}{T}\right)^m \left(\frac{\mu_d}{T}\right)^n \quad (4)$$

which defines the usual form of the QNS [3, 4]. Since the flavours are degenerate, the order of  $m$  and  $n$  does not matter; the coefficients with one of them vanishing are called the diagonal QNS. In the past we have constructed the Taylor expansion

$$\frac{\chi_{20}(T, \mu_B)}{T^2} = \frac{\chi^0(T)}{T^2} + \chi^2(T) \frac{\mu_B^2}{2!T^2} + \chi^4(T) T^2 \frac{\mu_B^4}{4!T^4} + \dots \quad (5)$$

and examined its divergence to obtain estimates of the critical end point [7, 15, 16]. Here we cross check this result using the Taylor expansion of eq. (3).

It is useful to recall that the various QNS at any given order have contributions from a variety of operator topologies [3], which can be constructed as follows. In the continuum theory, the operators contributing to any  $N$ -th order QNS have  $N$  insertions of  $\gamma_0$  connected in all possible ways by fermion propagators. The topologies track the number of insertions within each closed fermion loop; for example  $\mathcal{O}_{112}$  is a topology which contributes to  $N = 4$  and contains two fermion loops with one insertion each and one fermion loop with two insertions. These topologies also classify the lattice operators. As a result, any QNS can be written in the form

$$\chi_i = \sum_{\alpha=1}^M n_{i\alpha} \langle \mathcal{O}_\alpha \rangle, \quad (6)$$

where  $i$  is a labelling of the QNS,  $M$  is the number of distinct topologies of a QNS of that order,  $\alpha$  labels the topology, the expectation value denotes a connected part averaged over configurations, and an enumeration of  $n_{i\alpha}$  is given in [7]. This decomposition will turn out to be useful in analyzing errors.

### III. RESULTS

#### A. Errors in the QNS

Each QNS is the sum of the expectation values of a set of operators with different topologies as in eq. (6),

$$\chi_i = \sum_{\alpha=1}^M n_{i\alpha} \langle \mathcal{O}_\alpha \rangle = \sum_{\alpha=1}^M \langle Q_\alpha \rangle = u \cdot Q. \quad (7)$$

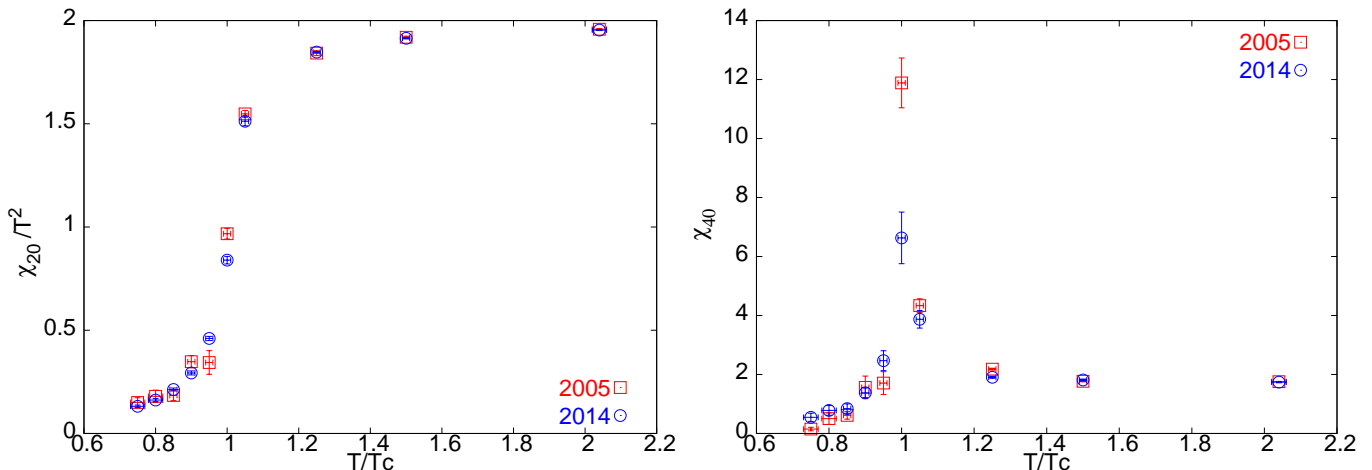


FIG. 3: Comparison of the new set B and old [7] extractions of the QNS of order 2 (first panel) and 4 (second panel). The largest effects are in the vicinity of  $T_c$  in both cases. By decreasing the number of source vectors in the analysis, we checked that the lower peak value of  $\chi_{40}$  in the current runs is due to increased  $N_v$ .

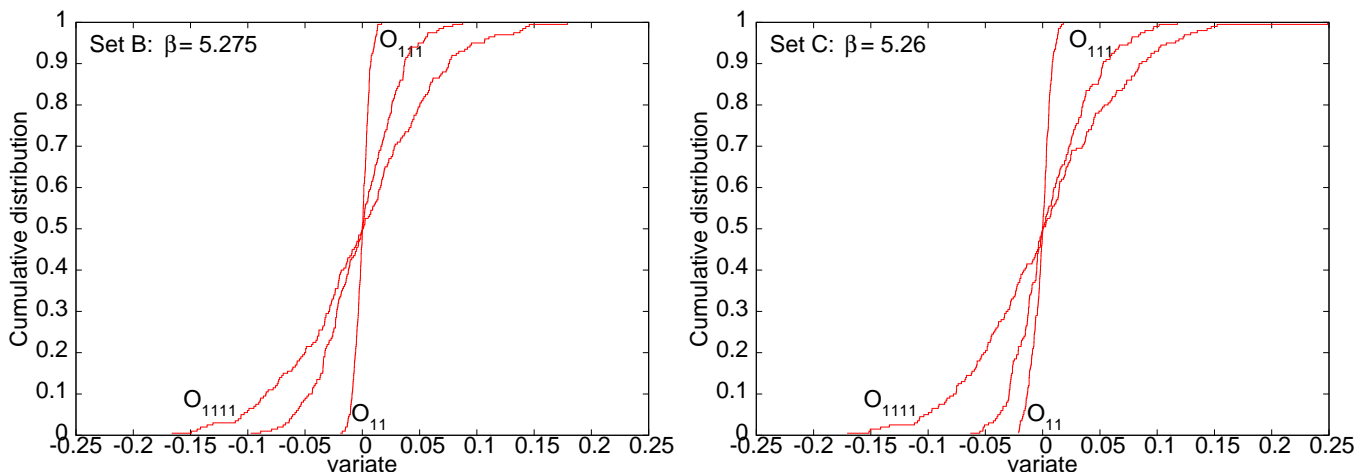


FIG. 4: Cumulative distributions of  $\mathcal{O}_{11}$ ,  $\mathcal{O}_{111}$  and  $\mathcal{O}_{1111}$ , evaluated by bootstrap and shifted such that the median is at zero. Note that, for both values of  $m_\pi/m_\rho$ , as the number of traces in the product increases, the tails of the distribution get fatter.

We have introduced the notation  $Q_\alpha = n_{i\alpha}\mathcal{O}_\alpha$ , as well as the  $M$ -dimensional vector  $Q$  whose  $\alpha$ -th component is  $\langle Q_\alpha \rangle$ . The  $M$ -dimensional vector  $u$  has all components equal to unity.

Some insight into which terms dominate the errors comes from a pseudo-Gaussian analysis. At each temperature, the largest components of  $Q$  dominate the expectation of a QNS. To find which terms dominate the error, we make a bootstrap estimate of the covariance matrix,  $\Sigma_{\alpha\beta}$  of the  $Q_\alpha$ ; its eigenvalues are  $\sigma_\gamma^2$  (ordered such that  $\gamma = 1$  is the largest) and the normalized eigenvectors are  $v_\gamma$ . If  $Q \cdot v_\gamma = |Q| \cos \theta_\gamma$ , then clearly

$$\chi_i = |Q| \sum_{\gamma=1}^M \cos \theta_\gamma u \cdot v_\gamma, \quad \text{and} \quad \text{Var } \chi_i = |Q|^2 \sum_{\gamma=1}^M \cos^2 \theta_\gamma (u \cdot v_\gamma)^2 \sigma_\gamma^2, \quad (8)$$

and the contribution of each term in the second sum defines which is the largest contributor to the error. The dominant terms in the two sums may not be the same. The analysis in terms of the covariance matrix would be exact if the errors were Gaussian. When the distributions of the variables are non-Gaussian, as here, the analysis still determines the most fluctuating directions in the neighbourhood of the mean.

Above  $T_c$  the contributions to the QNS are similar to that predicted by simple power counting [17]. The contributions to the errors are also dominated by the same operators. The situation below  $T_c$  is more complicated. Second order QNS are dominated both in magnitude and error by the contribution from  $\langle \mathcal{O}_2 \rangle$ , if it contributes. Fourth order

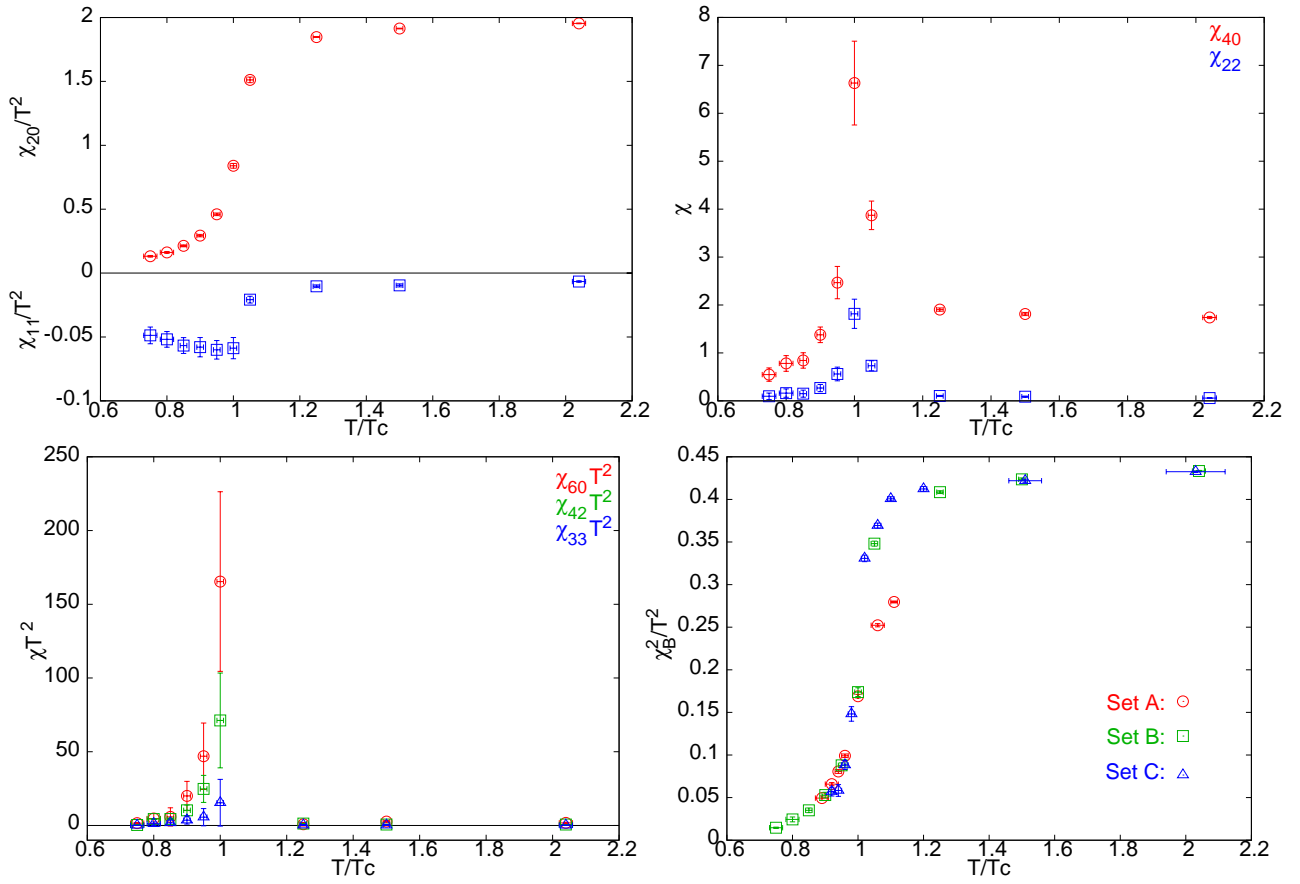


FIG. 5: QNS in set B. The first panel shows  $\chi_{20}/T^2$  (circles) and  $\chi_{11}/T^2$  (boxes) as functions of  $T/T_c$  on  $N_t = 4$  lattices. Notice the difference in scales for the two QNS. The second panel shows  $\chi_{40}$  (circles) and  $\chi_{22}$  (boxes) as a function of  $T/T_c$  for  $N_t = 4$  lattices. The third panel shows  $\chi_{60}T^2$  (circles),  $\chi_{42}T^2$  (boxes) and  $\chi_{33}T^2$  (triangles) as functions of  $T/T_c$ . The fourth panel shows  $\chi_B^2/T^2$  for the three sets.

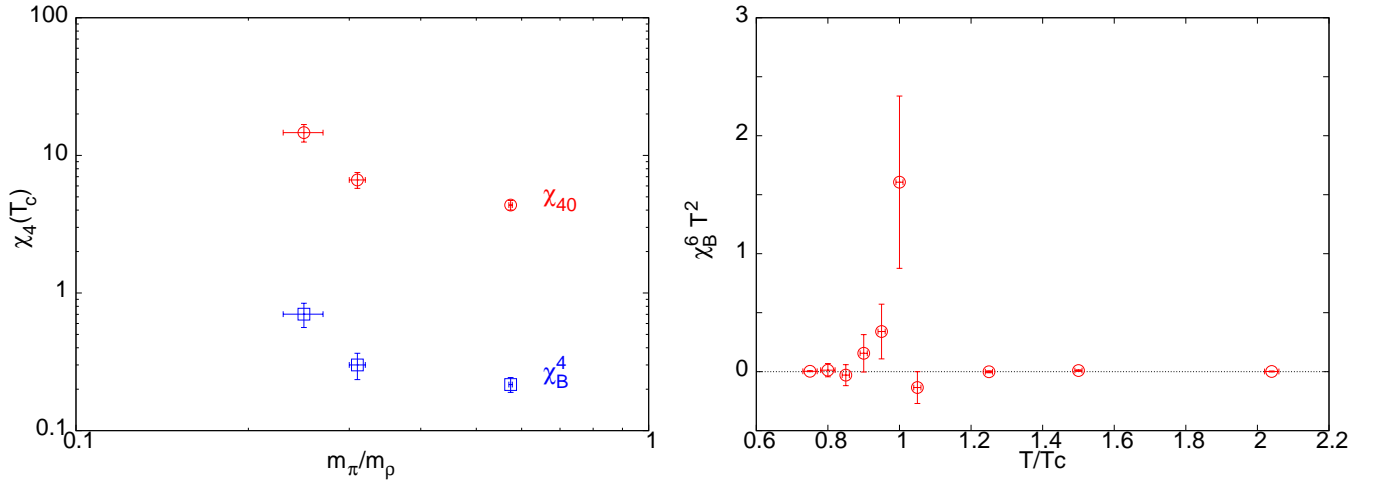


FIG. 6: The first panel shows the dependence of the peaks of two fourth order QNS as functions of  $m_\pi/m_\rho$ ; a power law does not seem to be a good descriptions. The second panel shows the dependence of  $\chi_B^6 T^2$  on  $T/T_c$  for set B. A peak is seen at  $T_c$ , where  $\chi_B^4$  also peaks.

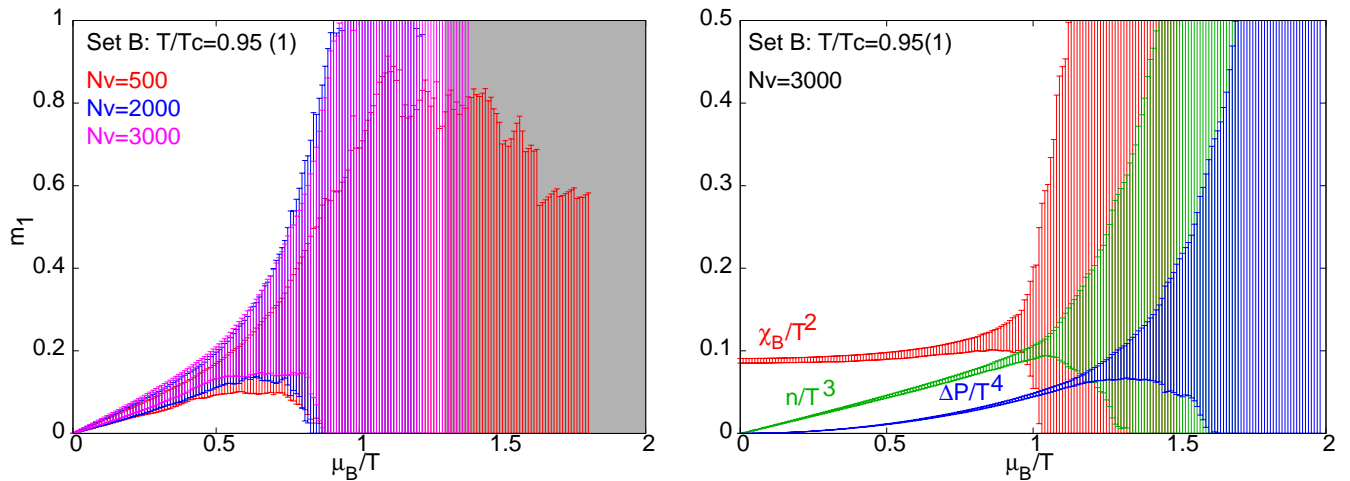


FIG. 7: The DLOG Padé approximant,  $m_1$ , and its errors are shown in the first panel; the dark band shows the radius of convergence obtained by analysis of the series coefficients. By successive integration one constructs  $\chi_B$ ,  $n$  and  $\Delta P$ , as shown in the second panel. The errors at different values of  $\mu_B/T$  are strongly correlated, and the reason for the decrease in errors with integration order is discussed in the text.

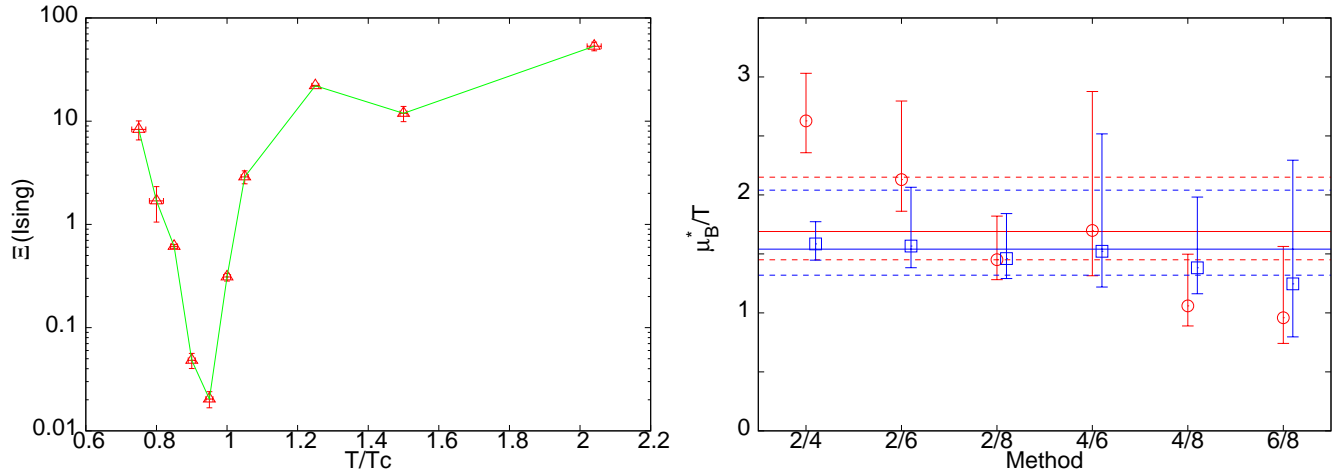


FIG. 8: The first figure gives a measure of the goodness of the DLOG Padé resummation assuming the critical behaviour to be in the Ising universality class in set B. We estimate  $T^E/T_c$  to be at the minimum of this curve. The second figure shows the radius of convergence obtained from the ratios of various terms in the series expansion of  $\chi_{20}$  (boxes) and the successive  $\chi_B^n$  (circles), obtained in set B. The best common value and its errors are marked by the bands.

QNS are dominated by the 2-loop operator  $\langle \mathcal{O}_{22} \rangle$  and the 3-loop operator  $\langle \mathcal{O}_{112} \rangle$ , the precise mix depending on the coefficients  $n_{i\alpha}$ . The errors generally come from just one eigenvector: that corresponding to the largest eigenvalue of the covariance matrix. In this, the 3-loop operator generally dominates, although the 4-loop  $\langle \mathcal{O}_{1111} \rangle$  has a significant contribution. Sixth order QNS have significant contributions from  $\langle \mathcal{O}_{222} \rangle$  and  $\langle \mathcal{O}_{1122} \rangle$ , the hierarchy being decided by the  $n_{i\alpha}$ . The errors are due essentially only to the leading eigenvector, which has major contributions from the  $\langle \mathcal{O}_{1122} \rangle$ ,  $\langle \mathcal{O}_{11112} \rangle$  and  $\langle \mathcal{O}_{111111} \rangle$ . Although a significant fraction of the error comes from operators whose contribution to the expectation is negligible, it does not seem possible to improve the errors except by throwing out “small” terms. Since this may introduce systematic errors, we do not explore this drastic solution.

The origin of large errors lies in the fact that the multi-loop operators are the products of individual loops. The measurement of each loop yields a random number with a distribution which depends on the bare parameters of the simulation. The distributions of products of random variates typically are non-Gaussian and have fat tails; we show some examples in Figure 4. Clearly more loops lead to fatter distributions. Unfortunately, distributions of products of random numbers have not received much attention in the literature. Examples in which the random variates are

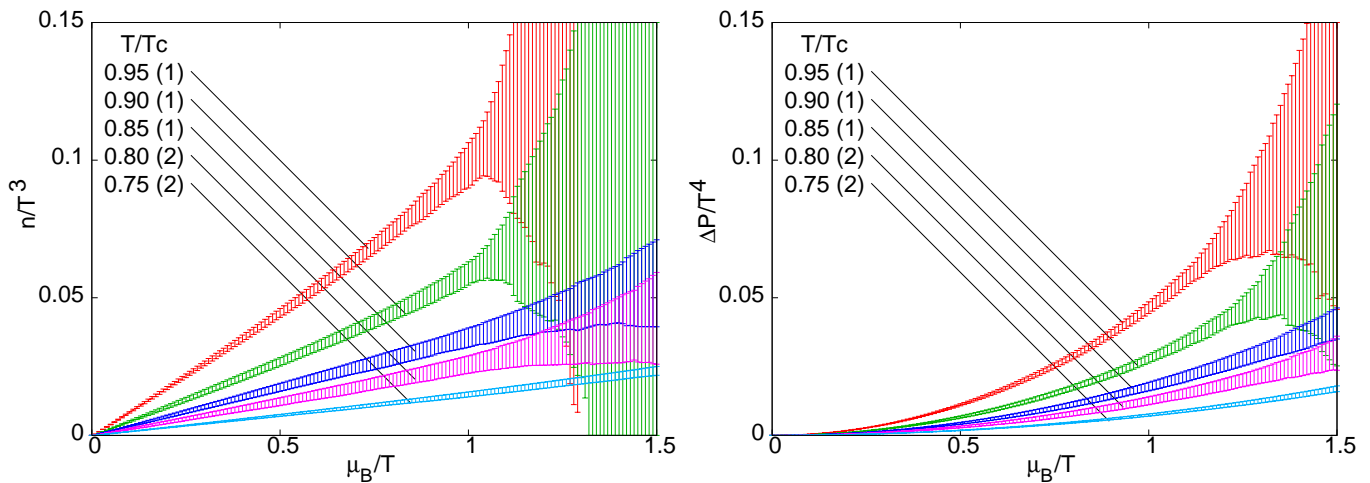


FIG. 9: The quark number density and the baryon contribution to the pressure as a function of  $\mu_B/T$  for various temperatures below and up to  $T_E$  in set B. The view as a function of  $T/T_c$  for several different  $\mu_B$  is shown in Figure 10.

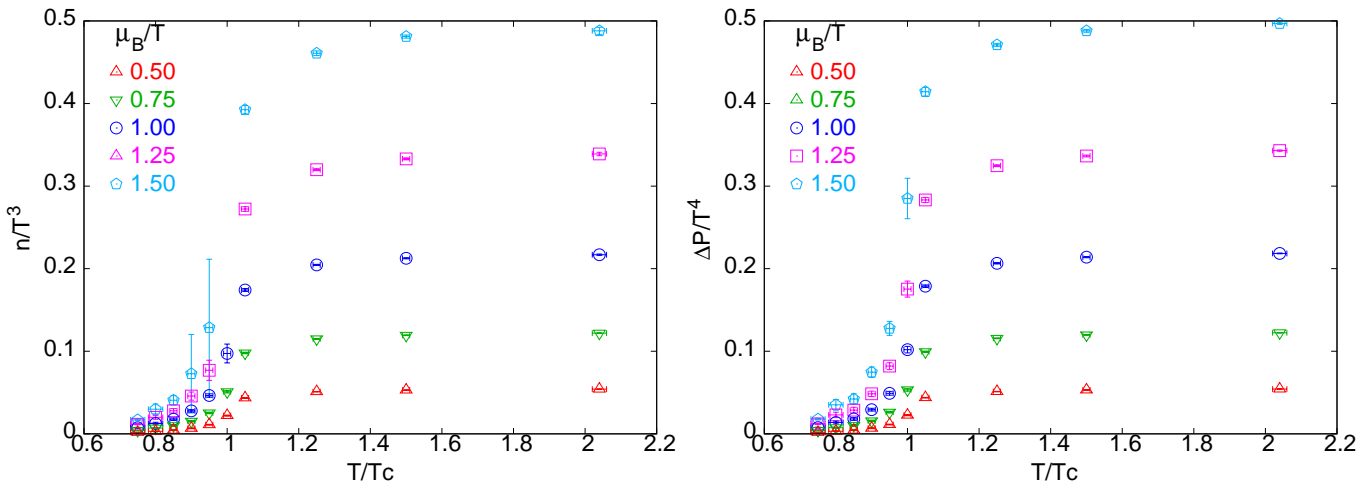


FIG. 10: The equation of state for set B shown as a function of  $T/T_c$  at various different values of  $\mu_B$ . The view as a function of  $\mu_B$  at several different  $T/T_c$  is given in Figure 9.

positive have been examined recently [18]. The case at hand is more complicated since the variates are of indefinite sign.

### B. The QNS and chiral critical behaviour

The second order QNS are shown in Figure 5. Smooth variations are seen as functions of  $T/T_c$  for both the QNS. The errors in the measurement of  $\chi_{11}/T^2$  are much reduced compared to previous measurements. As a result, we can clearly see a smooth temperature variation. Two of the fourth order QNS are also shown in Figure 5. Each has a sharp peak at  $T_c$ . We can trace this to a peak in  $\langle \mathcal{O}_{22} \rangle$  at  $T_c$ . We also find a sharp peak at  $T_c$  in the sixth order QNS, which is exhibited in Figure 5. This peak is not a statistical artifact since it develops into a stable value as  $N_v$  is increased to 2000.

The variation of the second order QNS with mass is displayed in the fourth panel of Figure 5. Below  $T_c$  the dependence of  $\chi_B^2/T^2$  on  $m_\pi$  seems to be statistically insignificant. At  $T_c$  and immediately above it, there is some dependence of this QNS on the quark mass. For set A  $m_\pi/T_c > 3$ , so the mass effect in the high temperature phase seems to be strong, and is likely to persist until fairly high  $T$ . For set B,  $m_\pi/T_c$  is less than half of this value, and we see that at  $1.5T_c$  sets B and C give similar results. The fourth order QNS have the form shown in Figure 5, with a

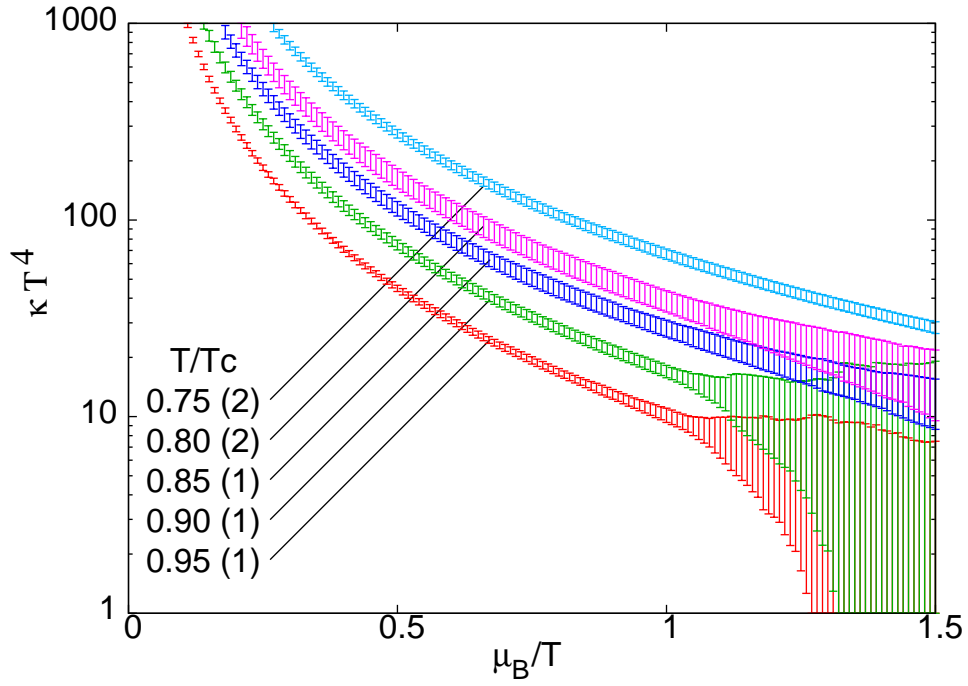


FIG. 11: The isothermal bulk compressibility in QCD as a function of the baryon chemical potential in set B.

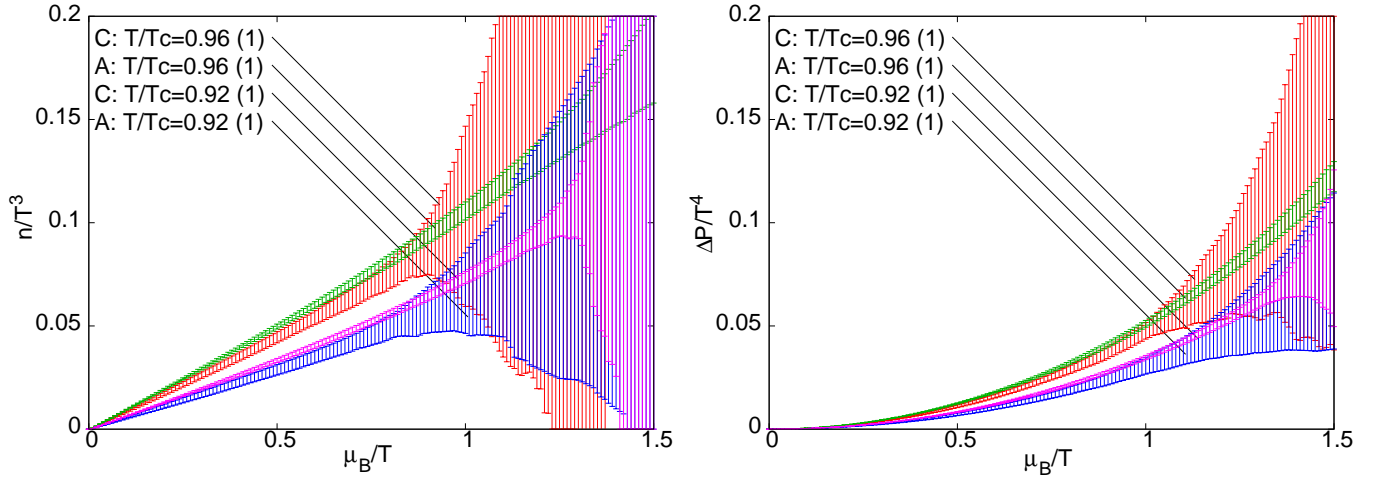


FIG. 12: The quark number density and the baryon contribution to the pressure at different temperatures and two different pion masses at each temperature. By comparing the two sets, one sees that the effect of the pion mass on the equation of state vanishes within errors over this range of pion masses.

peak at  $T_c$ . We find little mass dependence below  $T_c$ , and some at  $T_c$  and above, although sets B and C coincide for  $T \geq 1.5T_c$ .

It was conjectured earlier that the chiral critical behaviour for  $m_\pi = 0$  and  $\mu_B = 0$  yields a scaling form,  $f_s(t)$ , for the singular part of the free energy as a function of the variable

$$t = a \left( \frac{T}{T_c} - 1 \right) + b \left( \frac{\mu_B}{T_c} \right)^2, \quad (9)$$

where  $a$  and  $b$  are scale parameters [19]. Successive derivatives of  $f_s$  with respect to  $T$  are then proportional to

successive double derivatives with respect to  $\mu_B$ , *i.e.*

$$\chi_B^{2n}(T) = \left. \frac{\partial^{2n} f_s}{\partial \mu_B^{2n}} \right|_{\mu_B=0} \propto \left. \frac{\partial^n f_s}{\partial T^n} \right|_{\mu_B=0}. \quad (10)$$

A sharp rise in  $f_s$  across the chiral phase transition would then give a peak at  $T_c$  in  $\chi_B^4$  and an oscillatory  $\chi_B^6$  with a zero at  $T_c$ . Moving away from the chiral limit would still give similar, but rounded and shifted, features. Such observations would then connect the finite temperature chiral transition with the QCD critical point. Such a scaling formula would relate the fourth order QNS to the specific heat, and so predict a power-law rise of  $\chi_B^4$  as  $m_\pi/m_\rho$  decreases. The power can be read off from the formalism presented in [19].

This important conjecture has not been subjected to a direct test before. A first test is possible now since we have taken data with several values of  $m_\pi/m_\rho$ . In the first panel of Figure 6 we plot our measurements of the peak of  $\chi_B^4$  and  $\chi_{40}$  against  $m_\pi/m_\rho$ . A power law is not seen. One possible reason is that the peak of  $\chi_B^4$  is not related to  $f_s$ . For example, at the masses we studied, it could be that the free energy is not dominated by its singular chiral part,  $f_s$ , and a power law may emerge at smaller quark masses. In this case a future computation at realistic pion masses,  $m_\pi/m_\rho = 0.18$ , and smaller, would be needed to test eq. (9). Alternatively there could be finite-volume shifts in the peaks of  $\chi_B^4$  which spoil the apparent scaling. A future finite size scaling study would then be needed to test this alternative.

In the second panel of Figure 6 we show  $\chi_B^6$  in set B, since it has the best statistics. We see a peak at  $T_c$  instead of the zero which would be predicted by eq. (10). By changing  $N_v$  in our analysis we have checked that the peak is stable and not a statistical fluke. This observation also indicates that, in the mass range which we have explored, the assumption that the free energy is dominated by the singular term in the chiral limit, with the scaling variable of eq. (9), is not supported. Clearly, these first tests should be supplemented by more detailed studies in future.

### C. The logarithmic derivative and its errors

When the series expansion of a function has a finite radius of convergence, then summing the truncated series has uncontrolled systematic errors. One needs a method of resumming the infinite series which remains reliable even as the statistical errors decrease. Near the critical point  $\chi_B/T^2$  is expected to diverge as  $|\mu_B^2 - (\mu_B^E)^2|^{-\psi}$ . It turns out to be simpler to examine the logarithmic derivative of  $\chi_B$ ,

$$m_1(T, \mu_B) = \frac{\partial \log \chi_B}{\partial \mu_B} \simeq \frac{2\psi \mu_B}{\mu_B^2 - (\mu_B^E)^2}. \quad (11)$$

The last expression comes by substituting the critical form of  $\chi_B$  into the definition. The quantity  $m_1$  was initially introduced in this form to connect with experimental measurements of event-to-event fluctuations in the baryon number in heavy-ion collisions [6, 20]. The series resummation consists of converting the series for  $\chi_B$  into one for  $m_1$ , and then matching the simple-pole ansatz to it. This is known as a DLOG Padé approximant in the literature [21]. The scaling assumption, *i.e.*, a single power-law divergence of  $\chi_B$  may turn out to be oversimplified; corrections to scaling can also be incorporated into the analysis if future improvements in statistics make it necessary [21].

Statistical errors in the evaluation of  $m_1$  are described in Appendix A, where it is shown that a bootstrap procedure can give good control of errors except in the neighbourhood of the critical point. It is shown that with increasing statistics,  $N$ , one can only control the errors within a distance  $\mathcal{O}(1/\sqrt{N})$  of the critical point. The need of large statistics to control errors near a critical point is known as critical slowing down [22]. This observation reveals that the use of series expansions also suffers from this generic disease near a critical point.

In the first panel of Figure 7 we show the resummation of  $m_1$  for different number of source vectors,  $N_v$ . The effect of increasing statistics is most clearly visible in the decrease of errors in  $m_1$  for  $\mu_B/T < 0.75$ . For larger values of  $\mu_B/T$  it seems that substantially larger statistics will be needed to gain control of errors. An estimate can be made as follows. We find that  $m_1$  has 50% errors at  $\mu_B/T = 0.66$  with  $N_v = 2000$  and at  $\mu_B/T = 0.73$  with  $N_v = 3000$ . Then, using the scaling formulæ of Appendix A, this would mean that we would need  $N_v > 10000$  to reduce the errors to 50% at  $\mu_B/T = 1$ , if we assume that  $\mu_B^E/T^E = 1.5$ .

The second panel of Figure 7 shows the resummation of the QNS and the equation of state using the DLOG. The QNS is obtained by integrating and then exponentiating  $m_1$ . Then  $n$  and  $\Delta P$  are obtained by further integrations. The initial conditions needed are provided by the measurement of  $\chi_B$  at  $\mu_B = 0$  and by the conditions that  $n$  and  $\Delta P$  vanish at  $\mu_B = 0$ . We use the trapezoidal rule for these integrations, and tune the integration step size.

If the errors in  $m_1$  were simple uncorrelated point-wise errors, then the integration error would be just the sum in quadrature. This would result in large errors in  $\chi_B$ ,  $n$  and  $\Delta P$  close to the critical point. However, the errors in  $m_1$

come from the parameters. In order to understand errors in the integrals, recall that all the quantities are functions of  $|\mu_B^2 - (\mu_B^E)^2|$ , and are successive integrals of  $m_1$ . So the error,  $\delta\Delta P$ , in  $\Delta P$  can be written as

$$\left(\frac{\delta\Delta P}{\Delta P}\right)^2 \simeq n^2(\delta\mu_B^E)^2, \quad (12)$$

if we assume that the error,  $\delta\mu_B^E$ , in  $\mu_B^E$  gives the dominant contribution to  $\delta\Delta P$ . Since  $n$  is regular at the critical point, so is this error. These arguments indicate that as we take more integrals of  $m_1$ , the errors decrease, since the critical singularity becomes milder. This is clearly visible in Figure 7.

Also visible in Figure 7 is the fact that integration smooths out singularities. The divergence of  $m_1$  is clear, the milder divergence of  $\chi_B$  is less so, and the subtle changes in the slopes of  $n$  and  $\chi_B$  would take significantly more statistics to see clearly. Indeed, it is through the abrupt increase in errors, related to critical slowing down, that one can infer most easily the presence of a critical point.

#### D. Critical behaviour

Analysis of the series coefficients in the expansion of  $\chi_{20}$  gives the radius of convergence. When the series coefficients are all clearly positive, then the radius of convergence corresponds to a real singularity. It turns out that in all three sets of runs, the Taylor series at  $T/T_c \simeq 0.95$  has a rather clear signal of a singularity on the real  $\mu_B$  axis. This is confirmed by the DLOG Padé analysis.

The DLOG Padé analysis of the series expansions of  $\chi_{20}$  and  $\chi_B$  agree with each other. For set B we find that the poles lie off the real axis for  $T < 0.9T_c$  and  $T > T_c$ . In these temperature intervals  $\psi$  turns out to be negative. So, there is no critical point outside the range  $0.9T_c \leq T \leq T_c$ . Within this range the series expansion for the DLOG is best compatible with the single pole ansatz for  $T/T_c = 0.95 \pm 0.01$ .

From the residue of the DLOG Padé at the pole one should be able to extract the critical index. Unfortunately, the errors are much too large for us to be able to quote a value. However, at our estimate of the critical point we obtain a value of  $\psi$  compatible with that expected in a 3-d Ising model as well as the mean-field theory (see Appendix B). Also, at this point, if we constrain the critical index to its Ising value, the location of the pole of the resulting DLOG Padé approximant is compatible with the estimate from the ratios of Taylor coefficients.

An useful confirmatory test is the following. Assume that the series coefficients of the DLOG determined numerically from the QNS are  $D_i$ . Then equating this to the Padé approximant gives

$$D_0\mu + D_1\mu^3 + D_2\mu^5 + D_3\mu^7 + \dots \simeq \frac{2\psi\mu_B}{\mu_B^2 - (\mu_B^E)^2}, \quad (13)$$

Since there are only two parameters to be determined for the right hand side, a series of more than two terms for  $m_1$  can test whether the pole is a good ansatz for the resummation of the series for  $m_1$ . Doing this amounts to making a series expansion of the right hand of eq. (13) by synthetic division, yielding a series with coefficients  $P_i$ . Then one can check whether  $D_i - P_i$  vanishes within errors. A simple statistic for this test is

$$\Xi = \frac{E(D_i - P_i)^2}{\sigma(D_i - P_i)^2}, \quad (14)$$

where  $E$  denotes the expectation value, and  $\sigma$  the error. In Figure 8 we show  $\Xi$  obtained with the second term of the series for set B, when the first term is used to obtain  $\mu_B^E$  assuming that  $\psi = 0.79$ . Smaller values of  $\Xi$  indicate a good fit. If the distribution of the  $D_i$  and  $P_i$  were Gaussian, then  $\Xi$  would be  $\chi^2$ -distributed, and it would be natural for a good fit to have  $\Xi \simeq 1$ . However, both  $D_i$  and  $P_i$  are fat-tailed and strongly non-Gaussian, as we have discussed before, so the small values of  $\Xi$  at the minimum are not unnatural.

As one can see in Figure 8, the series expansion in set B indicates that the critical region lies in the range of temperatures  $0.9T_c \leq T \leq T_c$ , with  $T/T_c \simeq 0.95$ , being the most probable location of the critical point. The same range is selected out by the DLOG analysis of  $\chi_B$  as well as  $\chi_{20}$ , and whether  $\psi$  is fixed or allowed to vary.

Given these multiple indicators we estimate the position of the critical point in the following manner. First we find the temperature at which the resummation works best, using the  $\Xi$  measure introduced above. We do this with fixed and floating  $\psi$ . In each of the three sets at hand, the best temperature obtained by these tests coincides. This gives us  $T^E/T_c$ . At this temperature we examine whether the series coefficients are all positive; again in all three sets we find that they are. Then we use the ratios of various coefficients in the series expansion, as done in earlier computations, to obtain an estimate of the radius of convergence,  $\mu_B^E/T^E$ . We check that this is consistent with the position of the pole in the DLOG Padé analysis, as they are in the three sets we examine. The results are collected in Table III.

Set	$m_\pi/m_\rho$	$m_N/m_\rho$	$T^E/T_c$	$\mu_B^E/T^E$
A	$0.574 \pm 0.004$	$1.61 \pm 0.01$	$0.94 \pm 0.02$	$1.5_{-0.1}^{+0.2}$
B	$0.32 \pm 0.03$	$1.57 \pm 0.08$	$0.95 \pm 0.01$	$1.5_{-0.2}^{+0.5}$
C	$0.25 \pm 0.02$	$1.4 \pm 0.1$	$0.96 \pm 0.01$	$1.4_{-0.2}^{+0.4}$

TABLE III: The position of the critical end point obtained using methods discussed in the text for the three sets of runs we use in this paper. The ratios of hadron masses are taken from [13, 14].

There is no change in  $T^E/T_c$  obtained for set B when compared with the earlier results in [7], however there is a shift in  $\mu_B^E/T^E$  from the value  $1.1 \pm 0.2$  reported earlier to the value given in Table III. By repeating the analysis with  $N_v = 100$  we obtain results near the older value. This leads us to conclude that the shift is due to the increased  $N_v$  used in the current study. Over the range of masses we explored, a mild shift in the critical end point towards  $T_c$  and smaller  $\mu$  cannot be ruled out by the data. However, simple linear and quadratic fits show that extrapolations to the physical point  $m_\pi/m_\rho = 0.18$  do not change the location of QCD critical point significantly.

### E. The equation of state

Our results in set B for the bulk thermodynamic quantities,  $n$  and  $\Delta P$ , are shown in Figure 9. Both these bulk quantities increase monotonically with  $T$  and  $\mu_B$ , as expected. Away from our estimated critical point the errors are small. Even so, the truncated sum is consistent with the resummed value. As one approaches the critical point, the errors in both  $n$  and  $\Delta P$  increase, as discussed before. A view of the equation of state as a function of  $T/T_c$  for several different  $\mu_B$  is shown in Figure 10. Interestingly, the errors are also large at  $T_c$ . However, this is due to the large errors visible in the measurements of the QNS (see Figure 5), and not to the resummation.

$\chi_B$  is a thermodynamic response function, in that it determines the response of QCD matter to a change in  $\mu_B$ . QCD at finite  $\mu_B$  has another thermodynamic response function, namely the isothermal bulk compressibility,  $\kappa$ . See Appendix C for a definition. Our results for the equation of state allow us to determine  $\kappa$ . The results are shown in Figure 11.

We also investigated the effect of a change in the quark mass. In Figure 12 we compare  $n$  and  $\Delta P$  at two different  $T/T_c$ , for the two extreme quark masses. The figure shows that the effect of quark mass is hardly visible in the data. The scaling direction  $H$  could have been a mixture of the quark mass and the chemical potential, as discussed in Appendix B. The observation that the quark mass dependence of the pressure is statistically insignificant supports an interpretation that the scaling direction is close to  $\mu$ . As a result the order parameter, which is the conjugate thermodynamic variable, must be essentially  $n$ , with perhaps a small admixture of the chiral order parameter. This would further imply that  $\psi \simeq 0.79$ , with little correction. It would be interesting to extend these computations closer to the chiral and continuum limits to check whether there are systematic changes as one approaches the QCD tricritical point.

## IV. CONCLUSIONS

We have made a high statistics study of quark number susceptibilities in QCD with two flavours of light quarks, for three different sets of quark masses yielding  $m_\pi/m_\rho$  between about 0.6 and 0.25. This included a very high statistics set (set B) with quark mass tuned to give  $m_\pi/m_\rho \simeq 0.3$ , extending an earlier study [7]. The number of fermion source vectors used in the stochastic evaluation of traces is 2000 or more, which is 20 times larger than the number used earlier. For this set, the number of uncorrelated gauge configurations is also 3–4 times larger than before, being 200 now. The effect of such enhancement in statistics on thermal order parameters is shown in Figure 2.

The increased statistics allows us to increase the precision of our measurements, and thereby access new physics. The enhanced precision is very clearly seen even in the second order QNS; while these are consistent with previous measurements [7], the higher statistics gives smoother results with smaller errors. The fourth order QNS are also consistent with previous results, albeit with a lower peak at  $T_c$ . Both are shown in Figure 3.

We infer from Figure 6 that the values of  $\chi_{40}$  and  $\chi_B^4$  at the peak do not scale as a power of  $m_\pi/m_\rho$ . One could take this as an indication of the failure of at least one of two assumptions: that the QNS close to the physical pion mass are dominated by the singular part of the free energy in the chiral limit, or that the scaling in eq. (9) holds. Such a conclusion may be further reinforced by the observation of the sixth order QNS, shown in Figure 5, which peaks at  $T_c$  instead of vanishing. We have discussed that this preliminary conclusion needs to be tested in two ways.

Finite size scaling studies would provide more accurate tests of eq. (9). It would also be interesting to repeat these computations at lower quark masses to see what happens closer to the chiral limit.

The QNS can be analyzed to find a radius of convergence of the series expansion of  $\chi_{20}$  via a ratio test, and to infer the existence of a critical end point, as has been done before. We extend this analysis here, by noting that when the series diverges, then the truncated expansion cannot give a good estimate of the values of the QNS,  $n$ , and  $\Delta P$  near the radius of convergence. If the divergence is due to a critical point, then  $\chi_B \simeq (\mu^2 - \mu_B^E)^{-\psi}$ . The logarithmic derivative of  $\chi_B$ , which is called  $m_1$ , then has a pole. A Padé analysis of  $m_1$ , called a DLOG Padé analysis, can then be used to resum the series. Error propagation in this process is non-trivial, and is described in Appendix A. This DLOG Padé tests whether the divergence is due to a critical point in three ways— first by testing whether the pole is at real  $\mu_B$ , second by testing whether the singularity in  $m_1$  corresponds to a divergent  $\chi_B$ , and third by checking whether the series for  $m_1$  can indeed be summed into a single pole. We find all three criteria yield a signal of a critical point at the positions given in Table III. Extrapolations of our results to the physical value of  $m_\pi/m_\rho \simeq 0.18$  gives  $T^E/T_c \simeq 0.95$  and  $\mu_B^E/T^E \simeq 1.5$ . Although the errors are currently too large to extract a critical index,  $\psi$ , with any degree of precision, it is possible to check whether the Ising value,  $\psi = 0.79$  (see Appendix B) is consistent with the data. We find that it is, although the data is not yet able to distinguish between Ising and mean-field behaviour.

Integrating  $m_1$  once and exponentiating, one gets  $\chi_B$ . Integrating repeatedly, one gets the baryon density,  $n$ , and the excess pressure,  $\Delta P$ . These are shown in Figure 9 as functions of  $T$  and  $\mu_B$ . The equation of state is shown as a function of  $T/T_c$  at several different  $\mu_B$  in Figure 10. From these quantities it is also possible to extract the isothermal compressibility of QCD, which is shown in Figure 11. In the previous section we have described in detail the evidence for a power-law singularity in the second derivative of  $\Delta P$ , *i.e.*, the derivative of  $n$ . Our figures for the equation of state show how difficult it is to pick out such a mild singularity from a plot of the function.

In Figure 12 we showed that the effect of quark mass on the equation of state is smaller than the statistical errors. Along with our observation of the lack of chiral effects in the QNS, this implies that the scaling directions for the critical scaling function are close to the physical parameters  $T$ ,  $\mu$  and  $m_\pi$ , at least in the vicinity of the physical pion mass. Lattice computations of quantities such as this would be able to constrain effective theories of the QCD critical point.

These computations were carried out on the Cray XK6 of the Indian Lattice Gauge Theory Initiative in IACS, Kolkata and the Cray X1 in TIFR, Mumbai. SG would like to thank Saumen Datta, Rajiv Gavai and Rishi Sharma for discussions and the Department of Science and Technology, Government of India, for support under grant no. SR/S2/JCB-100/2011.

### Appendix A: Errors in Padé approximants

We would like to evaluate the  $[0, 1]$  Padé approximant

$$P(z; a) = \frac{1}{z - a}, \quad (\text{A1})$$

at various  $z$  when  $a$  is determined from lattice simulations with some errors. If  $a$  has Gaussian errors, then, no matter which  $z$  we choose, there is a non-vanishing probability that  $a = z$ . So the mean and variance of  $P$  both diverge. To see this, scale and shift  $z$  so that  $a$  is distributed as a Gaussian with mean 1 and variance  $\sigma^2$ . Then the probability distribution of  $P$  at any fixed  $z$  is given by

$$p(P; z) = \frac{1}{\sqrt{2\pi\sigma^2}} \frac{1}{P^2} e^{-(z-1-1/P)^2/(2\sigma^2)}. \quad (\text{A2})$$

The distribution is normalizable but none of its moments exist, which means that the values of the function  $P(z; a)$  are completely uncertain.

Fortunately, there is a meaningful way to regularize this problem and to obtain a finite value and error for the Padé approximant. The solution lies in recognizing that one always deals with finite statistics, so the maximum and minimum values of the Padé are always bounded. The analysis also leads us to a better understanding of the bootstrap procedure.

Suppose that the estimates of the expectation and errors in  $a$  are made with finite statistics,  $N$ . If one estimates the mean and error of  $P(z; a)$  by a bootstrap, then one should take the number of bootstrap samples to be  $\mathcal{O}(N)$ . In the bootstrap sample  $|z - a|$  has a minimum and a maximum value. The probability that the minimum value is exactly zero is vanishingly small. Then the maximum value of  $P$  is finite. By accounting for the restricted range  $|P| \leq \Lambda$ , all the integrals are regularized. If the measurements are made with statistics of  $N$ , then  $\sigma^2 \propto 1/N$ . In most samples of the bootstrap, one can find a  $\Lambda$  such that

$$\epsilon(\Lambda) = 1 - \int_{-\Lambda}^{\Lambda} dP p(P; z), \quad (\text{A3})$$

and  $N\epsilon(\Lambda) \ll 1$ . If so, then the problem is regularized for any fixed value of  $N$ , in the sense that the bootstrap estimation yields a finite mean and a finite variance for  $P(z; a)$ .

The next question is whether one can take the limit  $N \rightarrow \infty$  with  $\sigma^2 \propto 1/N$  and  $\epsilon \propto 1/N$  in such a way that the mean and variance of  $P$  remain bounded. To check this we note that with increasing  $N$  one can arrange  $N\epsilon$  to be constant by scaling  $\Lambda \rightarrow \zeta\Lambda$  with  $\zeta \propto N^{3/2}$ . For Gaussian distributed  $a$ , the change in the mean and variance when  $\zeta$  changes to  $\zeta'$  is

$$\begin{aligned} \delta\langle P \rangle &\simeq e^{-K(1-z)^2 N} \log(\zeta/\zeta') \\ \delta\langle P^2 \rangle &\simeq e^{-K(1-z)^2 N} (\zeta - \zeta') \Lambda \sigma \end{aligned} \quad (\text{A4})$$

As a result a bootstrap estimation will lead to bounded mean and error for the Padé approximant except when  $|z - 1| < \mathcal{O}(1/\sqrt{N})$ .

One can go beyond the Gaussian approximation for the distribution of  $a$ . The main idea is to bound the growth of  $\langle P \rangle$  and  $\langle P^2 \rangle$  by verifying that the estimate of the error in the pole narrows with  $N$  faster than the growth of the probability in the tail of the distribution of the value of  $P(z; a)$ .

### Appendix B: Widom scaling ansatz

Consider a system in which the order parameter,  $M$ , has a non-zero value only on one side of a temperature  $T = T_c$ . Widom scaling is the statement that the ordering field,  $H$ , the reduced temperature,  $t = T/T_c - 1$ , and  $M$  are related through a homogeneous function, of degree  $\beta\delta$ , which can be written in the form

$$H = |M|^\delta J \left( \frac{|t|}{|M|^{1/\beta}} \right). \quad (\text{B1})$$

The exponents  $\beta$  and  $\delta$ , and the function  $J$  define the universality class. Two simple observations follow. First, if the system has finite  $M$  for  $H = 0$ , for some  $t$ , then  $|t|/|M|^{1/\beta}$  must be fixed to be the value which gives  $J = 0$ . Then one has the scaling relation

$$|M| \propto |t|^\beta. \quad (\text{B2})$$

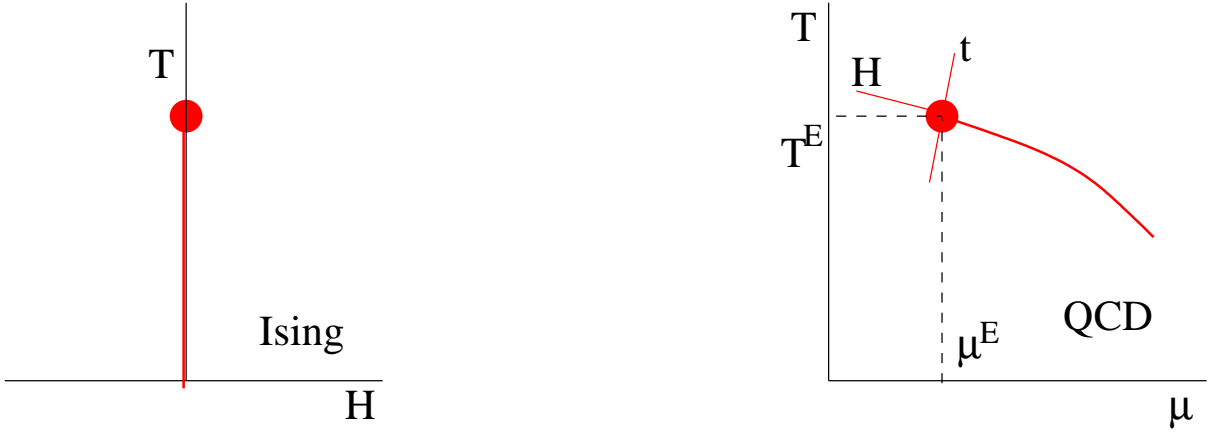


FIG. 13: The scaling directions  $t$  and  $H$  in the Ising model are parallel to the directions of physical temperature and magnetic field. In QCD, however, they may not coincide with  $T$  and  $\mu_B$  because the phase boundary is curved.

The second observation is that one can construct the order parameter susceptibility,  $\chi$ , by taking the derivative

$$\chi^{-1} = \left. \frac{\partial H}{\partial M} \right|_t = |M|^\delta \frac{J'}{\beta} \frac{|t|}{|M|^{1+1/\beta}}. \quad (\text{B3})$$

This is obtained using the chain rule and dropping the term in which the derivative lands on the prefactor of  $J$ , since  $J = 0$ .  $J'$  is the value of the derivative for the argument which gives  $J = 0$ . This immediately gives the Widom scaling formula

$$\chi \propto |t|^{-\gamma}, \quad \text{with} \quad \gamma = \beta(\delta - 1). \quad (\text{B4})$$

These scaling relations are well known.

Applying this to QCD, one would naturally want to interpret  $M = n - n_E$ , *i.e.*, the departure of the baryon density,  $n$ , from its value at the critical point. One could set  $t$  to be  $\Delta T$ , the difference between the temperature and its critical value in QCD and  $H$  to be,  $\Delta\mu_B$ , the difference between the chemical potential and its critical value in QCD. With this simple identification, one finds the QCD interpretation of the above critical exponents. However, in QCD, it is more interesting to examine small  $|t|$ , *i.e.*, the neighbourhood of the critical point. On doing this, one finds

$$M \propto H^{1/\delta}, \quad \text{and} \quad \chi \propto H^{-\psi} \quad \text{with} \quad \psi = 1 - \frac{1}{\delta}. \quad (\text{B5})$$

The continuity of pressure forces  $\psi$  to be less than unity. In the 3d Ising model,  $\beta = 0.33$  and  $\delta = 4.79$ , so one has  $\gamma = 1.24$  and  $\psi = 0.79$ . In the mean-field model,  $\delta = 3$ , which implies that  $\psi = 0.66$ .

In QCD there is no compelling reason to declare that the scaling directions  $t$  and  $H$  are coincident with the thermodynamic couplings  $\Delta T$  and  $\Delta\mu_B$ . The most general course of action would be to set  $t(\Delta T, \Delta\mu_B)$  and  $H(\Delta T, \Delta\mu_B)$ . When the arguments are small, the functions can be treated in a linear approximation, which corresponds to scaling (which is absorbed into a choice of units) and a rotation. So, in general  $t = \cos\phi\Delta T + \sin\phi\Delta\mu_B$  and  $H = \cos\phi\Delta\mu_B - \sin\phi\Delta T$ . The results of eq. (B5) we obtained by taking  $\phi = 0$ . Instead, if  $\phi = \pi/2$ , then  $t = \Delta\mu_B$  and  $H = -\Delta T$ , and the scaling formula becomes

$$|\Delta T| = |n|^\delta J \left( \frac{|\Delta\mu_B|}{|n|^{1/\beta}} \right). \quad (\text{B6})$$

Now the analogue of eq. (B2) is  $n \propto |\Delta\mu_B|^\beta$ . The scaling of  $\chi$  with  $\mu_B$  can be obtained by taking the variation of eq. (B6) with fixed  $\Delta T$  while varying  $n$  and  $\Delta\mu_B$  simultaneously:

$$d|\Delta T| = \delta|n|^{\delta-1} J dn + |n|^\delta J' \frac{d\Delta\mu_B}{|n|^{1/\beta}} - |n|^\delta J' \frac{\Delta\mu_B dn}{|n|^{1+1/\beta}}. \quad (\text{B7})$$

Taking this at  $J = 0$ , so that the above scaling holds, we find  $\psi = 1 + \beta = 1.33$ . The fact that the pressure must be continuous and finite across the critical point implies that  $\psi \leq 1$ . This rules out  $\phi = \pi/2$ . However, by varying the

angle  $\phi$  one can exhaust the range  $1 - 1/\delta \leq \psi \leq 1$ . The upper limit constrains the scaling direction  $H$  to be close to  $\mu_B$ .

More realistically, one should consider the phase diagram in the space of  $T$ ,  $\mu_B$  and the quark mass. In this extended space, the scaling directions may be rotated as above, leading to a mixing between the conjugate variables, the chiral condensate and the baryon density [11]. As above, this could also lead to an apparent departure from Ising value,  $\psi = 0.79$ . Then the number density would depend on  $m_\pi$  as the power  $2/\delta$ . In the Ising model  $2/\delta = 0.42$ , and in the mean field theory it is 0.66, so the dependence would be fairly strong.

### Appendix C: The isothermal bulk compressibility

For materials whose constituents move non-relativistically, the bulk compressibility,  $\kappa$ , is defined as

$$1/\kappa = -V \frac{\partial P}{\partial V}, \quad (\text{C1})$$

where the other thermodynamic quantities are held fixed as the pressure and volume are varied. Which quantities are held fixed defines the ensemble which should be used when computing it from the underlying theory. The most commonly used parameter is the isothermal bulk compressibility, which is defined at fixed particle number and temperature.

In a relativistic theory the particle number is not conserved, so the extension to QCD, especially at high-temperatures, requires the usual generalization: the canonical ensemble consists of states with fixed flavour quantum numbers, such as the baryon number,  $B$ . Thus, one may generalize the isothermal bulk compressibility to QCD matter by the definition

$$1/\kappa = -V \left. \frac{\partial P}{\partial V} \right|_{BT}. \quad (\text{C2})$$

The pure gauge theory has infinite  $\kappa$ ; when a gluon gas is compressed at fixed  $T$ , the pressure does not change. Defining  $\mu_B$  by the relation between the internal energy and the baryon number,  $dU = -\mu_B dB$ , when keeping everything else fixed, one may write

$$1/\kappa = V \frac{\partial P}{\partial \mu_B} \frac{\partial \mu_B}{\partial V} = n \mu_B, \quad (\text{C3})$$

where  $n$  is the baryon density. We use this equation to determine  $1/\kappa$ . When  $\mu_B$  and  $n$  are small then one can make the approximation  $n = \chi_B \mu_B$ , and  $\kappa n^2 = \chi_B$ . It is clear that this approximation fails as soon as the contribution of higher order QNS become appreciable. While this is not apparent from Figure 11, it is clear if one plots  $\kappa \mu_B^2$  against  $\mu_B$ .

- 
- [1] I. Arsene *et al.*, *Nucl. Phys. A* 757 (2005) 1; B. B. Back *et al.*, *Nucl. Phys. A* 757 (2005) 28; J. Adams *et al.*, *Nucl. Phys. A* 757 (2005) 102; K. Adcox *et al.*, *Nucl. Phys. A* 757 (2005) 184.
  - [2] H. Song, arXiv 1401.0079 (to appear in *Pramana*).
  - [3] R. V. Gavai and S. Gupta, *Phys. Rev. D* 68 (2003) 034506.
  - [4] S. Gottlieb *et al.*, *Phys. Rev. Lett.* 59 (1987) 2247.
  - [5] M. M. Aggarwal *et al.* (STAR Collaboration), *Phys. Rev. Lett.* 105 (2010) 022302;
  - [6] R. V. Gavai and S. Gupta, *Phys. Lett. B* 696 (2011) 459.
  - [7] R. V. Gavai and S. Gupta, *Phys. Rev. D* 71 (2005) 114014.
  - [8] A. Bazavov (HotQCD Collaboration) *Nucl. Phys. A* 904–905 (2013) 877c.
  - [9] S. Borsanyi *et al.*, *J. H. E. P.* 1011 (2010) 077.
  - [10] J. Berges and K. Rajagopal, *Nucl. Phys. B* 538 (1999) 215; M. A. Halasz *et al.*, *Phys. Rev. D* 58 (1998) 096007.
  - [11] D. T. Son and M. A. Stephanov, *Phys. Rev. D* 70 (2004) 056001.
  - [12] Y. Aoki *et al.*, *Nature* 443 (2006) 675; *ibid.*, *J. H. E. P.* 0906 (2009) 088.
  - [13] S. Gupta and N. Karthik, *Phys. Rev. D* 87 (2013) 094001.
  - [14] S. Gottlieb *et al.*, *Phys. Rev. D* 38 (1988) 2245.
  - [15] S. Datta, R. V. Gavai and S. Gupta, *Lattice* 2013.
  - [16] R. V. Gavai and S. Gupta, *Phys. Rev. D* 78 (2008) 114503.
  - [17] J.-P. Blaizot, E. Iancu and A. Rebhan, *Phys. Lett. B* 523 (2001) 143.

- [18] M. G. Endres *et al.*, *Phys. Rev. Lett.* 107 (2011) 201601.
- [19] B. Friman *et al.*, *Eur. Phys. J. C* 71 (2011) 1694.
- [20] S. Gupta, *PoS CPOD2009* (2009) 025.
- [21] D. S. Gaunt and A. J. Guttmann, p. 181, *Phase Transitions and Critical Phenomena*, Vol. 3, eds. C. Domb and M. S. Green, Academic Press, London, 1974.
- [22] P. C. Hohenberg and B. I. Halperin, *Rev. Mod. Phys.*, 49 (1977) 435.